ADVANCED FUNCTIONAL MATERIALS
www.afm-journal.de

4D Printed Protein-AuNR Nanocomposites with Photothermal Shape Recovery

Siwei Yu, Naroa Sadaba, Eva Sanchez-Rexach, Shayna L. Hilburg, Lilo D. Pozzo, Gokce Altin-Yavuzarslan, Luis M. Liz-Marzán, Dorleta Jimenez de Aberasturi, Haritz Sardon,* and Alshakim Nelson**

4D printing is the 3D printing of objects that change chemically or physically in response to an external stimulus over time. Photothermally responsive shape memory materials are attractive for their ability to undergo remote activation. While photothermal methods using gold nanorods (AuNRs) are used for shape recovery, 3D patterning of these materials into objects with complex geometries using degradable materials is not addressed. Here, the fabrication of 3D printed shape memory bioplastics with photo-activated shape recovery is reported. Protein-based nanocomposites based on bovine serum albumin (BSA), poly (ethylene glycol) diacrylate (PEGDA), and AuNRs are developed for vat photopolymerization. These 3D printed bioplastics are mechanically deformed under high loads, and the proteins served as mechano-active elements that unfolded in an energy-dissipating mechanism that prevented fracture of the thermoset. The bioplastic object maintained its metastable shape-programmed state under ambient conditions. Subsequently, up to 99% shape recovery is achieved within 1 min of irradiation with near-infrared (NIR) light. Mechanical characterization and small angle X-ray scattering (SAXS) analysis suggest that the proteins mechanically unfold during the shape programming step and may refold during shape recovery. These composites are promising materials for the fabrication of biodegradable shape-morphing devices for robotics and medicine.

1. Introduction

The combination of shape memory materials with additive manufacturing has led to the field of 4D printing, which is the 3D printing (or additive manufacturing) of objects that can change chemically or physically over time, in response to an external stimulus.[1–6] Nature inspires 4D printed materials with increasingly complex form factors (shapes) and has the ability to sense and respond to exogenous inputs from the environment.[7–10] Additive manufacturing techniques that use material extrusion,[11–14] or vat photopolymerization,[15–17] processes have vastly improved over the last decade and enable complex geometries to be fabricated based on a computer-aided design file.[18–20] While 4D printing is applicable to soft robotics and biomedical devices, new materials are still required for the future, particularly where the life cycle of the printed structures must also be taken into consideration.[21,22]

S. Yu, N. Sadaba, E. Sanchez-Rexach, A. Nelson
Department of Chemistry
University of Washington
Seattle, WA 98195, USA
E-mail: alshakim@uw.edu

N. Sadaba, E. Sanchez-Rexach, H. Sardon
POLYMAT and Department of Polymers and Advanced Materials: Physics Chemistry, and Technology
Faculty of Chemistry
University of Basque Country UPV/EHU
Donostia-San Sebastián 20018, Spain
E-mail: haritz.sardon@ehu.eus

S. L. Hilburg, L. D. Pozzo
Department of Chemical Engineering
University of Washington
Seattle, WA 98195, USA

G. Altin-Yavuzarslan
Molecular Engineering and Sciences Institute
University of Washington
Seattle, WA 98195, USA

L. M. Liz-Marzán, D. Jimenez de Aberasturi
CIC biomaGUNE
Basque Research and Technology Alliance (BRTA)
Donostia-San Sebastián 20014, Spain
E-mail: djimenezdeaberasturi@cicbiomagune.es

L. M. Liz-Marzán, D. Jimenez de Aberasturi
Biomedical Networking Center on Bioengineering Biomaterials and Nanomedicine (CIBER-BBN)
Donostia-San Sebastián 20014, Spain

L. M. Liz-Marzán, D. Jimenez de Aberasturi
Ikerbaque
Basque Foundation for Science
Bilbao 48009, Spain

The ORCID identification number(s) for the author(s) of this article can be found under https://doi.org/10.1002/adfm.202311209

DOI: 10.1002/adfm.202311209

Photothermal activation has received significant attention for programming and recovery of shape memory polymers (SMPs).[23–30] Broadly, the photo-activation of SMPs is categorized as being direct or indirect. In direct light activation, the polymer photochemically responds to light, as has been observed for cis-trans isomerization of azobenzene.[31] Indirect light activation (as is the case for photothermal activation) is dependent upon the conversion of light into a second form of energy, such as heat.[32] In this case, the thermal energy locally increases the temperature of the material above its glass transition temperature (T_g), to facilitate the shape recovery.[23] Carbon nanotubes,[33] graphene,[34] and metal nanoparticles (NPs) such as plasmonic gold NPs (AuNPs),[9,13,17,18] are widely used as photothermal converters. Resonant light interactions with AuNPs can lead to high photothermal efficiency and use as nano-heaters.[38,39] Photothermal activation has significant advantages over direct light or heat activation because it can achieve more uniform heat distribution within a 3D printed body. As a result, shape recovery can be faster, while still enabling remote and spatial control over the recovery process.[40]

Stereolithographic apparatus (SLA) 3D printing and other vat photopolymerization techniques have been used to pattern SMPs into 4D objects that respond to light.[23,40–45] For example, Wang et al.[23] and Paunović et al.[45] have shown vat photopolymerization 3D printing of photothermal-responsive SMP by incorporating AuNPs into the polymer network. The localized surface plasmon resonances of gold nanostructures are highly dependent upon their size and shape and determine the wavelength of light at which the photothermal response occurs. Thus, investigating anisotropic nanostructures, such as AuNRs, can further expand the utility of 4D printed structures.

Degradable SMPs are of interest for applications where biodegradation or end-of-use considerations are important. Well-established examples SMPs include polylactic acid (PLA),[46–49] poly(e-caprolactone) diacrylate (PCL-DA),[50] and polyvinyl alcohol (PVA).[51] Silk fibroin methacrylate (Sil-MA),[52,53] BSA-based hydrogels,[54] and BSA/PEGDA[55] have all been reported as SMPs. The BSA-PEGDA SMPs are particularly interesting because the printed bioplastic constructs are enzymatically degradable thermosets, and they exhibit plasticity due to the mechanical unfolding of the BSA proteins in the network.[56,57] Thus, the constructs are mechanically programmed into a metastable shape when placed under a mechanical load. The original shape of the construct can be subsequently recovered by thermal treatment. However, prolonged recovery times at temperatures above 100 °C may also cause BSA proteins to denature during the recovery process, which results in altered mechanical properties for the recovered construct.

Herein, we demonstrate 3D printed protein-based nanocomposites with remote photothermal shape recovery. AuNRs with longitudinal localized surface plasmon resonance (LSPR) around 795 nm were selected as highly efficient photothermal sensitizers and incorporated into resins, to afford a polymer network comprising BSA/PEGDA and methacrylate bovine serum albumin (MABSA)/PEGDA with dispersed AuNRs. The non-hydrated cross-linked networks exhibit plasticity as a consequence of the mechanical unfolding of the BSA. As a result, 3D printed bioplastic composites can be mechanically deformed into a metastable shape, and subsequently photothermally recovered upon illumination with NIR light. We demonstrate that photothermal shape recovery offers several advantages due to the rapid, localized, and homogeneous heating: i) the shape recovery is fast (within 1 min) and ii) the mechanical properties are nearly identical to the original after shape recovery, which suggests that the mechanism for shape recovery is coupled to some level of protein refolding within the network.

2. Results and Discussion

In this work, we investigated BSA/PEGDA and MABSA/PEGDA resins with AuNRs for SLA 3D printing and characterized the mechanical and thermal characteristics of these materials. The major component of the resins was either BSA or MABSA (**Figure 1a**). We previously reported BSA/PEGDA resin formulations[55] that utilize *aza*-Michael addition of the acrylate functionalities to BSA surface lysine, to form a BSA/PEGDA prepolymer. We have also reported MABSA/PEGDA formulation[57] where over 90% of the surface lysine groups on BSA were converted into methacrylamide derivatives to form MABSA. Both resin formulations afford protein-polymer networks during the 3D printing process. We investigated resins with protein/PEGDA ratios of 3:1 and 2:1, using either BSA or MABSA as the protein source. The total solid content in the resin from the protein and PEGDA was 40 wt.% in the aqueous solution (60 wt.% DI water), and 1 wt.% lithium phenyl-2,4,6-trimethylbenzoylphosphinate (LAP) was added to each of the formulations. The amount of AuNRs in the resins varied from 0.001 to 0.002 wt.% with respect to the total resin formulation including water. The complete composition for each formulation is summarized in Table S1 (Supporting Information).

The AuNRs used were coated with thiolated polyethylene glycol (PEG-SH) as a surface stabilizer (supporting information), thereby ensuring stability in aqueous mixtures[58] and compatibility with the surrounding polymer matrix. Figure S3b (Supporting Information) shows the UV-NIR spectrum of the synthesized AuNRs in water, with two distinct peaks at 795 and 509 nm, corresponding to longitudinal and transverse LSPR modes of the AuNRs, respectively. Transmission electron microscopy (TEM) images show the same AuNRs are 60 nm in length and 15 nm in width with no aggregation, high monodispersity, and well-defined rod-like shape.

The suitability of the AuNR-containing resins for SLA 3D printing to form bioplastics was first evaluated, based on viscosity and the rate of photocuring. Based on our previous studies, resins should have viscosities less than 10 Pa·s to facilitate reflow and minimize capillary forces during the printing process.[55] The viscosities of the 16 different formulations tested in this study were below 1 Pa·s (Figure S1, Supporting Information). Additionally, the photopolymerization kinetics of the resin were studied using photorheology, wherein changes in both the storage and loss moduli were monitored upon irradiation with 365 nm light. The rapid increase in the storage modulus upon irradiation is indicative of a resin suitable for SLA 3D printing (Figure S2, Supporting Information). The presence of the AuNRs did not affect the viscosity and photo-curing rate of the resin. All the resins were printed on a commercially available Form 2 printer. The aqueous resin formulations tested in this study generate water-swollen

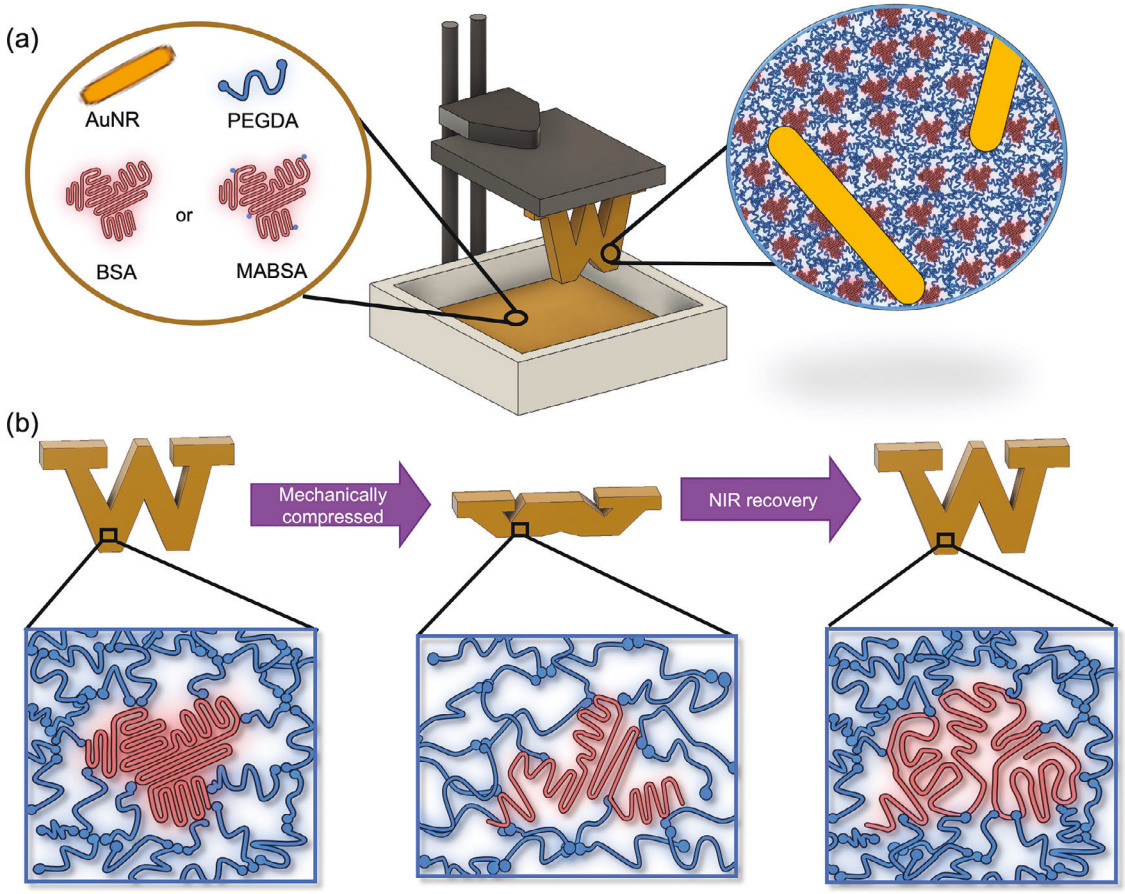

Figure 1. a) Illustration of the SLA 3D printing of aqueous BSA or MABSA resins with PEGDA and AuNRs, and a molecular-level depiction of the printed protein-polymer network. b) General scheme for the workflow of shape programming and recovery. The 3D printed constructs are first dehydrated to afford bioplastics that can be mechanically compressed to program a new metastable shape, which remains stable under ambient conditions for an indefinite period of time. Irradiation of the metastable construct with an NIR laser leads to rapid recovery of the original shape. The cartoon networks show the proposed conformations of BSA: the native-like globular structure of the original bioplastic construct, the outstretched form in the metastable construct, and the non-native-like globular structure of the shape-recovered construct.

hydrogels. Therefore, the 3D printed constructs must first be dehydrated for 48 h to afford their bioplastic form. Deswelling was observed to be isotropic,[55] and the average change in volume was approximately 57%. This drying method consistently afforded a residual water content of 5.5 wt.% for BSA/PEGDA bioplastics with different concentrations of AuNRs, see Figure S14 (Supporting Information).

The workflow for shape deformation and photothermal recovery is illustrated in Figure 1b. First, the printed bioplastic construct was compressed on a load frame with a 50 kN load cell to 70% strain for the BSA/PEGDA formulations and 60% strain for the MABSA formulations. The mechanically programmed constructs are metastable and maintained their deformed state for an indefinite period (over a year) under ambient conditions, see Figure S13 (Supporting Information). The printed construct is a thermoset, i.e. a cross-linked protein-polymer network, and thus, the plasticity of this material is highly unusual.[59] We attribute this behavior to the mechanically induced unfolding of the globular proteins[60,61] in the network to release its stored length.[62,63] The compressed structures were then subjected to irradiation using an 808 nm NIR laser with a power of 3.75 W cm^{-2}. Heating the sample above the T_g of the network-enabled rapid shape recovery, typically being complete within 3 min.

Differential scanning calorimetry (DSC) was used to determine the glass transition temperature (T_g) of the bioplastics with different BSA/PEGDA and MABSA/PEGDA ratios (each of these samples contained 0.00375 wt.% AuNRs relative the mass of the bioplastic). The T_g values for BSA/PEGDA 2:1 and 3:1 were 46.21 and 50.13 °C, while those for MABSA/PEGDA 2:1 and 3:1 were 38.06 and 42.63 °C, respectively. The T_g of a miscible mixture can be predicted by Flory-Fox equation, which is based on the weight fraction of the components.[64] Since both BSA and MABSA have a higher T_g than that of PEGDA (700 g mol^{-1}), the T_g values increased as the concentration of protein was increased in the network and were consistent with the theoretical predictions (see Supporting Information). Additionally, we observed lower T_g values for MABSA-based bioplastics compared to BSA-based bioplastics, which might be attributed to the difference in surface functionalization. Both BSA/PEGDA 2:1 and MABSA/PEGDA 3:1 exhibited $T_g \approx 40$ °C, which could potentially be used as applications under physiological conditions because their T_g is slightly

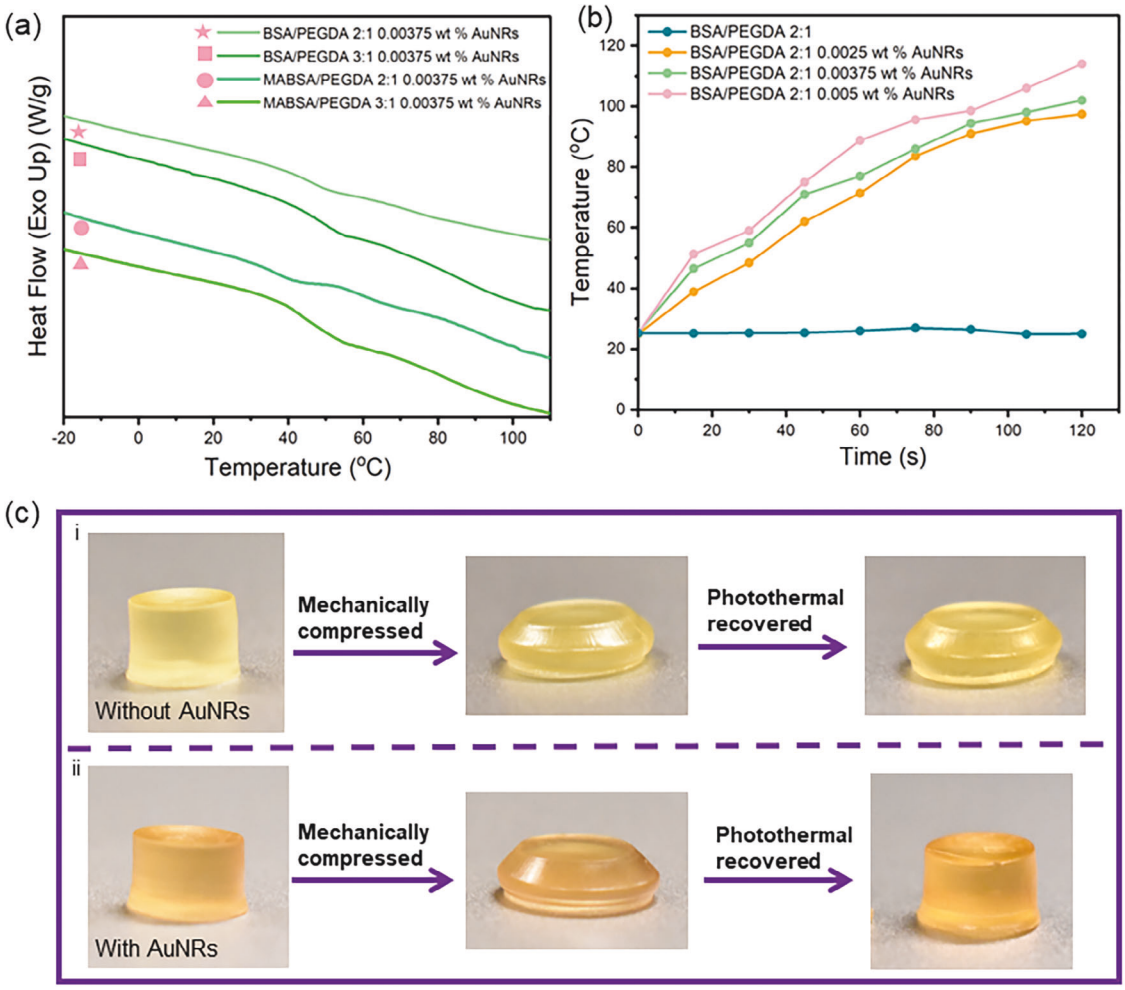

Figure 2. a) DSC curves for protein-PEGDA bioplastic composites with 0.0035 wt.% AuNRs. b) Graph showing the change in temperature with irradiation time for BSA/PEGDA 2:1 with varying amounts of AuNRs. c) Comparison of the compression and recovery of a cylindrical disk with a BSA/PEGDA 2:1 composition (i) without AuNRs and (ii) with AuNRs (0.005 wt.%). The dimension of the original cylinder was 8.3 mm × 5.2 mm and the compressed sample was 3.2 mm × 11.8 mm.

higher than human body temperature; however, further research needs to be conducted to assess the functionality of the bioplastic under these conditions. We also investigated the change in temperature as a function of irradiation time for BSA/PEGDA 2:1 with 0–0.005% AuNRs (**Figure** 2b). The samples with 0.00375 and 0.005 wt.% AuNRs exceeded the T_g of the respective material within 20 s. On the other hand, reducing the AuNRs amount to 0.0025 wt.% required 30 s to exceed the T_g. The control sample without AuNRs did not show a noticeable temperature increase after NIR laser irradiation, which demonstrates that the photothermal effect was solely due to the AuNRs.

The mechanical shape programming and photothermal shape recovery were evaluated for 3D printed cylinders from BSA/PEGDA 2:1 (Figure 2c), BSA/PEGDA 3:1, MABS/PEGDA 2:1 and 3:1 (Table S3, Supporting Information). First, the cylindrical constructs were compressed to 70% of their original height for BSA-based and 60% for MABSA-based bioplastic to afford the metastable form of the construct. Then, recovery was achieved through irradiation with the NIR laser. The compression was performed at ambient temperature, which makes the process more convenient and energy-saving compared to traditional SMPs that require programming of the temporary structure by heating above its T_g and then fixing the temporary shape by cooling down below the T_g.[23] The shape recovery for BSA/PEGDA 2:1 began after 10 s of irradiation and was complete within 2 min. The percent shape recovery was determined by measuring the height of the cylinder before and after laser recovery. The recovery for a printed disk of BSA/PEGDA 2:1 with AuNRs was about 96 ± 3% after 2 min of irradiation with an NIR laser at 3.75 W cm^{-2} power, Figure 2c.

Uniaxial compression experiments were conducted to determine the mechanical properties of BSA/PEGDA and MABSA/PEGDA bioplastics with varying concentrations of AuNRs (**Figure** 3b). We observed that the compressive moduli for the samples remained unchanged upon incorporation of AuNRs. We compared the mechanical responses of different ratios of BSA/PEGDA and MABSA/PEGDA compositions, in the absence of AuNRs (Figure 3c). The compressive moduli for BSA/PEGDA 2:1, BSA/PEGDA 3:1, MABSA/PEGDA 2:1, and MABSA/PEGDA 3:1 was 132.5 ± 6.2, 168.0 ± 5.2,

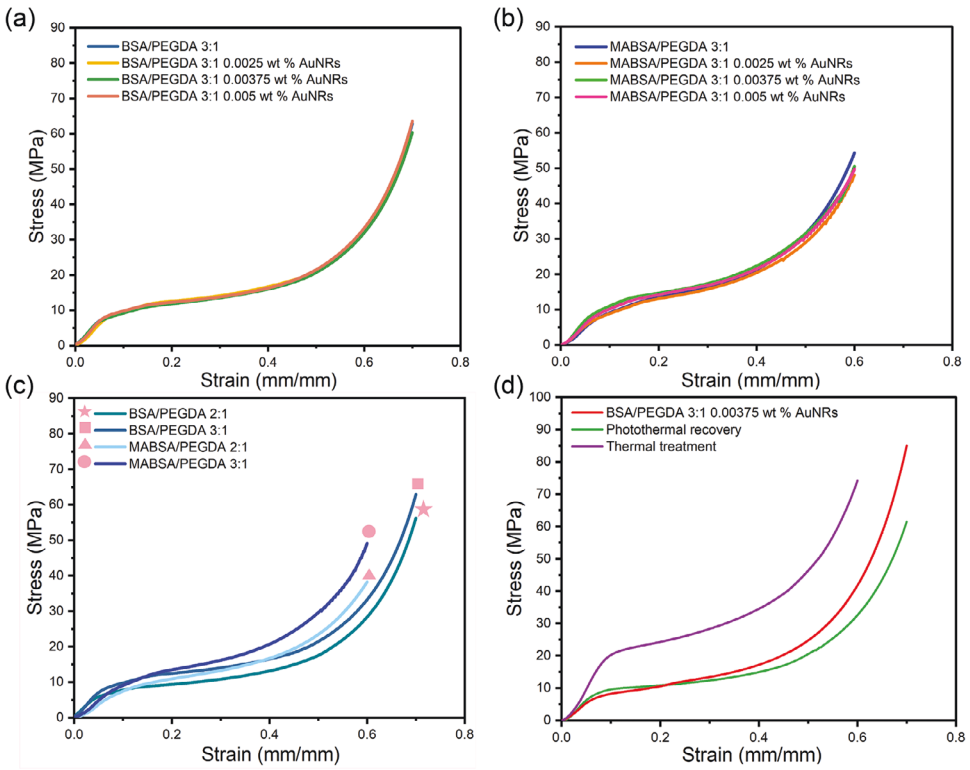

Figure 3. Compressive stress versus strain curves of 3D printed bioplastics a) BSA/PEGDA 3:1 bioplastics with 0–0.005% AuNRs, b) MABSA/PEGDA 3:1 bioplastic with 0-0.005% AuNRs, c) 4 different formulated bioplastics without gold nanorod, d) BSA/PEGDA 3:1 0.00375% AuNRs bioplastics compare with its laser-recovered bioplastic (red) or heat treatment (120 °C for 30 min) bioplastic (purple).

108.3 ± 6.7, and 141.2 ± 6.3 MPa, respectively. In general, as the concentration of the protein increased in the network, the compressive modulus also increased. The graphs indicate that the compressive moduli were nearly identical before and after NIR laser-induced recovery (Figures 3d; Figure S7, Supporting Information). In contrast, there is an increase in the compressive modulus in the heat-treated sample. These results agree with our previous report[55] wherein these thermal curing conditions (120 °C for 30 min) resulted in a higher compressive modulus. For the thermal treatment sample, the proteins in the network were thermally denatured as evidenced by the presence of an amide stretching band in the IR spectrum, which is consistent with beta-sheet like structures. In principle, heating the bioplastic above 90 °C using the NIR laser would cause the deformation of BSA secondary structure, as it is known to denature above 90 °C, both in solution and solid state.[21,65] The emergence of these secondary structures also increased the elastic modulus and decreased the ductility of the shape-recovered construct.[55,66] We hypothesize that the AuNRs dispersed in the biopolymer matrix provide rapid but uniform, local heating. The time required for shape recovery was short, and an amide stretching band for beta-sheet like structures was not observed in the infrared spectrum (Figure S4, Supporting Information). Instead, we only observed a peak at 1648 cm^{-1}, which is consistent with the alpha-helical secondary structure in BSA.

We further examined this structural evolution using small-angle X-ray scattering (SAXS) to assess changes at the nanoscale. Although both thermal and photothermal recovery of the shape can be rapid, the degree of protein unfolding and possibly refolding after shape recovery are different. A feature at $q \approx 0.11$ $Å^{-1}$corresponding to real space dimensions of 5.7 nm, which is approximately the size of the BSA protein, is present in the initial bioplastic. We observed no sharp peak for BSA under dilute conditions in its scattering profile (Figure S15). However, in the case of our BSA bioplastic networks, there is a very high concentration of BSA (75% by weight) that is surrounded by a PEG shell. Therefore, in such a concentrated state, we expect strong structure factor S(q) effects to cause stronger correlation peaks. The peak observed in the SAXS plot corresponds to a characteristic distance of ≈5.7 nm, which is consistent with the size of BSA. This peak likely originates from strong correlations between BSA proteins within the bulk material. We observed that after disappearing upon compression, this feature partially reemerges after laser recovery, as seen in **Figure 4**. In contrast, after thermal recovery, this feature is no longer visible, and a broad feature ranging q value of approximately 0.04–0.10 $Å^{-1}$ becomes prominent instead. This change indicates a loss of structural order as compared to the sharp feature present in the initial bioplastic. Although a smaller, broad feature is also visible in the laser-recovered sample, it is far less prominent, and the laser-recovered sample maintains more structural similarity to the starting sample.

Based on these results, we propose a mechanism for BSA as mechanoresponsive junctions within the network, as shown in Figure 1b. During compression, BSA junctions are mechanically unfolded to release their stored length. The presence of

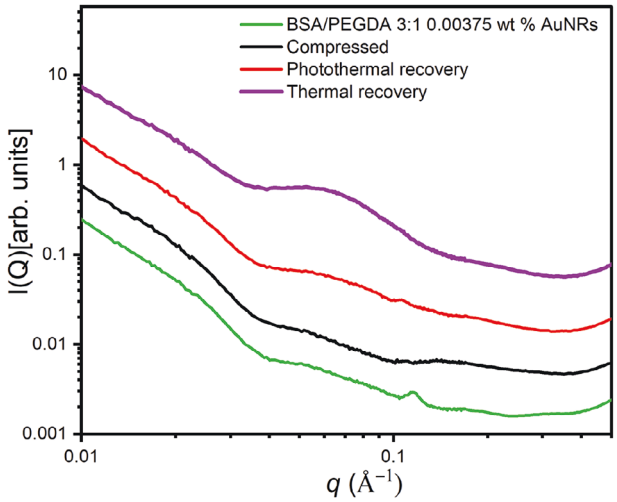

Figure 4. SAXS plots for BSA/PEGDA 3:1 composites with (0.00375 wt.% AuNRs).

the permanent PEGDA covalent junctions provides the network with memory that facilitates photothermal shape recovery. The presence of the 5.7 nm feature in the SAXS plot recorded from the shape-recovered construct suggests that globular, folded BSA junctions are present in the network. We were unable to determine from SAXS whether the BSA was refolded back into its native form or into another misfolded structure. These data are consistent with uniaxial compression studies (Figure 3d), wherein the linear elastic and plateau regions of the stress–strain curves were found to be similar for the first and second compression experiments. The difference in the densification region may arise from a greater number of interactions between neighboring protein molecules. Additional studies are underway to further understand the conformational states of the proteins within these networks.

Photoactivation using NIR wavelengths is advantageous due to the high penetration depth of NIR light.[67] To demonstrate shape recovery through a thicker structure, a solid spherical ball (D = 7.7 mm) was 3D printed using the BSA/PEGDA 3:1 resin with AuNRs. While this spherical structure can easily roll around, after this construct is compressed, the flattened sphere can no longer roll. Photothermal shape recovery can recover the metastable structure back to its spherical form, which thereby regains its ability to roll (Figure S11, Video S1, Supporting Information). The photothermal performance of a 3D printed bioplastic was further investigated by performing a shape recovery experiment while irradiating through a sheet of gelatin (thickness = 3.5 mm), as an analog for animal tissue (**Figure 5a**). The 808 nm NIR laser can penetrate through the gelatin to photothermally heat the metastable structure and regain 99% of the spherical shape within 1 min.

Shape recovery was also demonstrated in a stepwise manner with localized, selective NIR irradiation. The petals (11 mm × 6 mm × 1 mm) of a 3D printed flower were folded 90° into a metastable shape (Figure 5b). Each petal could then be independently unfolded back to its original shape by exposing it to NIR light (Figure 5b). These results show that multiple metastable states can be achieved with selective spatial irradiation with the laser.

3. Conclusion

In conclusion, we developed a photothermally responsive shape memory material via the incorporation of AuNRs into protein-polymer networks. The 3D printed bioplastic composites comprising BSA/PEGDA or MABSA/PEGDA polymer networks were fabricated in a vat photopolymerization process to afford a range of different 3D shapes. Once dehydrated, these objects could be mechanically programmed into a metastable secondary shape, which was maintained for an indefinite period of time. We photothermally recovered the original shape by irradiating the metastable construct with NIR light (808 nm). Despite the relatively small concentration of AuNRs in the composite (0.001 – 0.002 wt.%), the sparse presence of AuNRs was sufficient to enable the homogeneous localized photothermal heating for rapid

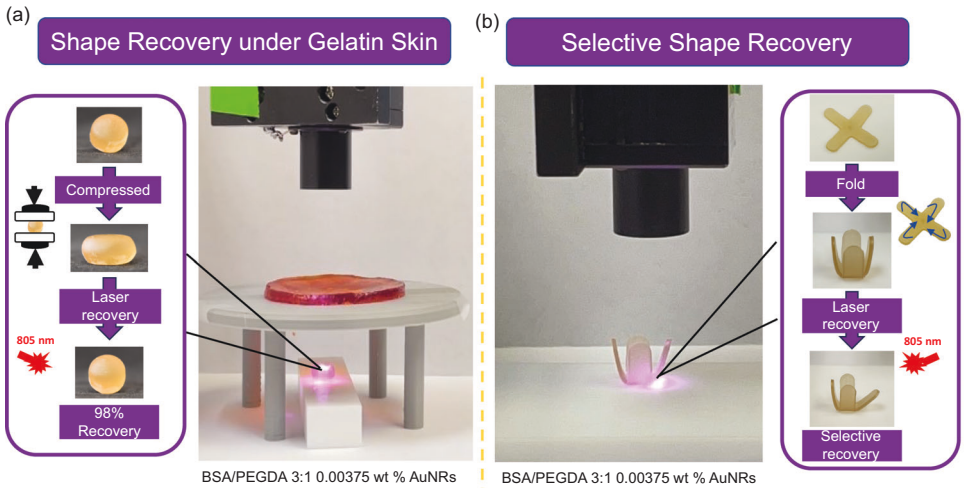

Figure 5. a) Shape recovery of BSA/PEGDA 3:1 0.00375 wt.% AuNRs 3D printed bioplastic ball under the pork gelatin skin. b) Selective shape recovery of folded 3D-printed BSA/PEGDA 3:1 0.00375 wt.% AuNRs 3:1 four arms flower.

shape recovery. We tuned the T_g of the bioplastics by changing the protein to polymer ratio. The protein content for both BSA- and MABSA-based bioplastics was as high as 75% by weight, and we achieved 90–99% shape recovery within 3 min of NIR irradiation.

While there are reports of 4D printing with protein-based materials to afford shape memory constructs, our work shows that BSA/PEGDA and MABSA/PEGDA composites with AuNRs possess a unique ability to exhibit a photothermal response as a bioplastic and in the absence of water. The mechanism is based on the mechanical unfolding of the BSA proteins in the network during the shape programming step and refolding of the proteins during photothermal shape recovery. Based on our SAXS data and mechanical characterization, we propose that the proteins refold and organize as globular shapes after heating above their T_g, but the exact conformation of these proteins is not known. Interestingly, the mechanical properties were similar after photothermal shape recovery in a subsequent compression cycle, which suggests that the proteins regained a globular form during the recovery step.

The implementation of NIR irradiation to recover the shape is advantageous because the protein-polymer matrix does not absorb at this wavelength and enables a larger depth of light penetration through the bioplastic. As a specific example, we demonstrated the penetration of NIR through pork gelatin as simulated tissue to afford 99% shape recovery within 1 min. Furthermore, the use of a NIR laser affords spatial control over the regions of irradiation. As a result, we could selectively fold the petals of a printed flower in a sequential manner. These materials have great potential as a biodegradable network for 4D printing for future biomedical devices.

Supporting Information

Supporting Information is available from the Wiley Online Library or from the author.

Acknowledgements

This research was financially supported by the Center for the Chemistry of Molecularly Optimized Networks (MONET), a National Science Foundation (NSF) Center for Chemical Innovation (CHE-2116298). Research reported in this publication was also supported by the National Institute of Biomedical Imaging and Bioengineering of the National Institutes of Health under award number R21EB031256. E.S-R. and H.S. acknowledge the European funding by the Marie Sklodowska-Curie Individual Fellowships (MSCA-IF-GF) 841879-4D Biogel. N.S. is grateful to the University of the Basque Country (UPV/EHU) and the Margarita Salas fellowship for the requalification of the Spanish University system for 2021–2023, financed by the European Union-Next Generation EU. The authors acknowledge the use of facilities and instrumentation supported by the U.S. National Science Foundation through the Major Research Instrumentation (MRI) program (DMR-2116265) and the UW Molecular Engineering Materials Center (MEM-C), a Materials Research Science and Engineering Center (DMR-1719797).

Conflict of Interest

The authors declare no competing interests.

Author Contributions

S.Y. and N.S. contributed equally to this project. S.Y., N.S., E.S-R., and A.N. conceived the project and designed the experiment. A.N., H.S., and D.J.A. oversaw the project. D.J.A. synthesized AuNRs. S.L.H. collected SAXS data. S.Y. wrote the manuscript with contributions from all authors. All authors have given approval to the final version of the manuscript.

Data Availability Statement

The data that support the findings of this study are available from the corresponding author upon reasonable request.

Keywords

3D printing, gold nanorod, photothermal, protein, shape recovery

Received: September 15, 2023
Revised: December 9, 2023
Published online: December 24, 2023

[1] X. Kuang, D. J. Roach, J. Wu, C. M. Hamel, Z. Ding, T. Wang, M. L. Dunn, H. J. Qi, *Adv. Funct. Mater.* **2019**, *29*, 1805290.
[2] M. Rafiee, R. D. Farahani, D. Therriault, *Adv. Sci.* **2020**, *7*, 1902307.
[3] A. Mitchell, U. Lafont, M. Hołyńska, C. Semprimoschnig, *Addit. Manuf.* **2018**, *24*, 606.
[4] F. Momeni, S. M. Mehdi Hassani N, X. Liu, J. Ni, *Mater. Des.* **2017**, *122*, 42.
[5] S. Tibbits, *Archit. Des.* **2014**, *84*, 116.
[6] A. Andreu, P.-C. Su, J.-H. Kim, C. S. Ng, S. Kim, I. Kim, J. Lee, J. Noh, A. S. Subramanian, Y.-J. Yoon, *Addit. Manuf.* **2021**, *44*, 102024.
[7] S. Schwarze, F. U. Zwettler, C. M. Johnson, H. Neuweiler, *Nat. Commun.* **2013**, *4*, 2815.
[8] S. Choi, K. Y. Lee, S. L. Kim, L. A. Macqueen, H. Chang, J. F. Zimmerman, Q. Jin, M. M. Peters, H. A. M. Ardoña, X. Liu, A.-C. Heiler, R. Gabardi, C. Richardson, W. T. Pu, A. R. Bausch, K. K. Parker, *Nat. Mater.* **2023**, *22*, 1039.
[9] D. Jang, L. E. Beckett, J. Keum, L. T. J. Korley, *J. Mater. Chem. B* **2023**, *11*, 5594.
[10] M. J. Glassman, J. Chan, B. D. Olsen, *Adv. Funct. Mater.* **2013**, *23*, 1182.
[11] J. M. Taylor, H. Luan, J. A. Lewis, J. A. Rogers, R. G. Nuzzo, P. V. Braun, *Adv. Mater.* **2022**, *34*, 2108391.
[12] J. Wong, A. Basu, M. Wende, N. Boechler, A. Nelson, *ACS Appl. Polym. Mater.* **2020**, *2*, 2504.
[13] A. Basu, J. Wong, B.o Cao, N. Boechler, A. J. Boydston, A. Nelson, *ACS Appl. Mater. Interfaces* **2021**, *13*, 19263.
[14] L. Li, Q. Lin, M. Tang, A. J. E. Duncan, C. Ke, *Chem. – Eur. J.* **2019**, *25*, 10768.
[15] S. Deng, J. Wu, M. D. Dickey, Q. Zhao, T. Xie, *Adv. Mater.* **2019**, *31*, 1903970.
[16] K. C. H. Chin, J. Cui, R. M. O'dea, T. H. Epps, A. J. Boydston, *ACS Sustainable Chem. Eng.* **2023**, *11*, 1867.
[17] C. Kasprzak, J. R. Brown, K. Feller, P. J. Scott, V. Meenakshisundaram, C. Williams, T. Long, *ACS Appl. Mater. Interfaces* **2022**, *14*, 18965.
[18] B. Narupai, A. Nelson, *ACS Macro Lett.* **2020**, *9*, 627.
[19] M. A. S. R. Saadi, A. Maguire, N. T. Pottackal, M. S. H. Thakur, M. M. Ikram, A. J. Hart, P. M. Ajayan, M. M. Rahman, *Adv. Mater.* **2022**, *34*, 2108855.
[20] F. P. W. Melchels, J. Feijen, D. W. Grijpma, *Biomaterials* **2010**, *31*, 6121.
[21] E. Sanchez-Rexach, T. G. Johnston, C. Jehanno, H. Sardon, A. Nelson, *Chem. Mater.* **2020**, *32*, 7105.

[22] E. M. Maines, M. K. Porwal, C. J. Ellison, T. M. Reineke, *Green Chem.* **2021**, *23*, 6863.
[23] Y. Wang, E. Sachyani Keneth, A. Kamyshny, G. Scalet, F. Auricchio, S. Magdassi, *Adv. Mater. Technol.* **2022**, *7*, 2101058.
[24] L. Ma, J. Wang, D. Zhang, Y. Huang, L. Huang, P. Wang, H. Qian, X. Li, H. A. Terryn, J. M. C. Mol, *Chem. Eng. J.* **2021**, *404*, 127118.
[25] L. Fang, T. Fang, X. Liu, Y. Ni, C. Lu, Z. Xu, *Compos. Sci. Technol.* **2017**, *152*, 190.
[26] H. Cui, S. Miao, T. Esworthy, S.-J. Lee, X. Zhou, S. Y. Hann, T. J. Webster, B. T. Harris, L. G. Zhang, *Nano Res.* **2019**, *12*, 1381.
[27] L. Fang, S. Chen, T. Fang, J. Fang, C. Lu, Z. Xu, *Compos. Sci. Technol.* **2017**, *138*, 106.
[28] Y. Chen, X. Zhao, C. Luo, Y. Shao, M.-B. Yang, B. Yin, *Compos. Part Appl. Sci. Manuf.* **2020**, *135*, 105931.
[29] J. Yang, J. Gong, L. Tao, Z. Tang, Z. Yang, P. Cao, Q. Wang, T. Wang, H. Luo, Y. Zhang, *Polym. J.* **2022**, *54*, 697.
[30] S.-T. Li, X.-Z. Jin, Y.-W. Shao, X.-D. Qi, J.-H. Yang, Y. Wang, *Eur. Polym. J.* **2019**, *116*, 302.
[31] L. Ceamanos, Z. Kahveci, M. López-Valdeolivas, D. Liu, D. J. Broer, C. Sánchez-Somolinos, *ACS Appl. Mater. Interfaces* **2020**, *12*, 44195.
[32] K. Jiang, D. A. Smith, A. Pinchuk, *J. Phys. Chem. C* **2013**, *117*, 27073.
[33] S. S. Mahapatra, S. K. Yadav, B. H. Lee, J. W. Cho, *Polymer* **2019**, *160*, 204.
[34] J. Loomis, X. Fan, F. Khosravi, P. Xu, M. Fletcher, R. W. Cohn, B. Panchapakesan, *Sci. Rep.* **2013**, *3*, 1900.
[35] Y. Wang, R. Yin, L. Jin, M. Liu, Y. Gao, J. Raney, S. Yang, *Adv. Funct. Mater.* **2023**, *33*, 2210614.
[36] H. Zhang, Y. Zhao, *ACS Appl. Mater. Interfaces* **2013**, *5*, 13069.
[37] N. Yenpech, V. Intasanta, S. Chirachanchai, *Polymer* **2019**, *182*, 121792.
[38] D. J. De Aberasturi, A. B. Serrano-Montes, L. M. Liz-Marzán, *Adv. Opt. Mater.* **2015**, *3*, 602.
[39] G. Baffou, R. Quidant, *Laser Photonics Rev.* **2013**, *7*, 171.
[40] A. Cortés, A. Cosola, M. Sangermano, M. Campo, S. González Prolongo, C. F. Pirri, A. Jiménez-Suárez, A. Chiappone, *Adv. Funct. Mater.* **2021**, *31*, 2106774.
[41] C. A. Spiegel, M. Hackner, V. P. Bothe, J. P. Spatz, E. Blasco, *Adv. Funct. Mater.* **2022**, 2110580.
[42] L. Wang, F. Zhang, S. Du, J. Leng, *ACS Appl. Mater. Interfaces* **2023**, *15*, 21496.
[43] Y. Y. C. Choong, S. Maleksaeedi, H. Eng, J. Wei, P.-C. Su, *Mater. Des.* **2017**, *126*, 219.
[44] A. Li, A. Challapalli, G. Li, *Sci. Rep.* **2019**, *9*, 7621.
[45] N. Paunovic, J. Marbach, Y. Bao, V. Berger, K. Klein, S. Schleich, F. B. Coulter, N. Kleger, A. R. Studart, D. Franzen, Z. Luo, J.-C. Leroux, *Adv. Sci.* **2022**, *9*, 2200907.
[46] X. Hao, J. Kaschta, X. Liu, Y. Pan, D. W. Schubert, *Polymer* **2015**, *80*, 38.
[47] Y. Liu, W. Zhang, F. Zhang, J. Leng, S. Pei, L. Wang, X. Jia, C. Cotton, B. Sun, T.-W. Chou, *Compos. Sci. Technol.* **2019**, *181*, 107692.
[48] T. M. Filion, J. Xu, M. L. Prasad, J. Song, *Biomaterials* **2011**, *32*, 985.
[49] F. S. Senatov, K. V. Niaza, M. Y. Zadorozhnyy, A. V. Maksimkin, S. D. Kaloshkin, Y. Z. Estrin, Z. Estrin, *J. Mech. Behav. Biomed. Mater.* **2016**, *57*, 139.
[50] F. O. Beltran, C. J. Houk, M. A. Grunlan, *ACS Biomater. Sci. Eng.* **2021**, *7*, 1631.
[51] Z. Fang, Y. Kuang, P. Zhou, S. Ming, P. Zhu, Y. Liu, H. Ning, G. Chen, *ACS Appl. Mater. Interfaces* **2017**, *9*, 5495.
[52] S. H. Kim, Y. B. Seo, Y. K. Yeon, Y. J. Lee, H. S. Park, M. T. Sultan, J. M. Lee, J. S. Lee, O. J. Lee, H. Hong, H. Lee, O. Ajiteru, Y. J. Suh, S.-H. Song, K.-H. Lee, C. H. Park, *Biomaterials* **2020**, *260*, 120281.
[53] A. Bucciarelli, M. Petretta, B. Grigolo, L. Gambari, A. M. Bossi, F. Grassi, D. Maniglio, *Gels* **2022**, *8*, 833.
[54] L. R. Khoury, I. Popa, *Nat. Commun.* **2019**, *10*, 5439.
[55] E. Sanchez-Rexach, P. T. Smith, A. Gomez-Lopez, M. Fernandez, A. L. Cortajarena, H. Sardon, A. Nelson, *ACS Appl. Mater. Interfaces* **2021**, *13*, 19193.
[56] G. Altin-Yavuzarslan, S. M. Brooks, S.-F. Yuan, J. O. Park, H. S. Alper, A. Nelson, *Adv. Funct. Mater.* **2023**, *33*, 2300332.
[57] P. T. Smith, B. Narupai, J. H. Tsui, S. C. Millik, R. T. Shafranek, D.-H. Kim, A. Nelson, *Biomacromolecules* **2020**, *21*, 484.
[58] C. García-Astrain, E. Lenzi, D. Jimenez De Aberasturi, M. Henriksen-Lacey, M. R. Binelli, L. M. Liz-Marzán, *Adv. Funct. Mater.* **2020**, *30*, 2005407.
[59] T. P. A. Hernandez, A. R. Mills, H. Yazdani Nezhad, *Compos. Struct.* **2021**, *261*, 113289.
[60] K. Makyla, C. Müller, S. Lörcher, T. Winkler, M. G. Nussbaumer, M. Eder, N. Bruns, *Adv. Mater.* **2013**, *25*, 2701.
[61] J. N. Brantley, C. B. Bailey, J. R. Cannon, K. A. Clark, D. A. Vanden Bout, J. S. Brodbelt, A. T. Keatinge-Clay, C. W. Bielawski, *Angew. Chem., Int. Ed.* **2014**, *53*, 5088.
[62] Z. Wang, X. Zheng, T. Ouchi, T. B. Kouznetsova, H. K. Beech, S. Av-Ron, T. Matsuda, B. H. Bowser, S. Wang, J. A. Johnson, J. A. Kalow, B. D. Olsen, J. P. Gong, M. Rubinstein, S. L. Craig, *Science* **2021**, *374*, 193.
[63] Z. Chen, J. A. M. Mercer, X. Zhu, J. A. H. Romaniuk, R. Pfattner, L. Cegelski, T. J. Martinez, N. Z. Burns, Y. Xia, *Science* **2017**, *357*, 475.
[64] S. Pásztor, B. Becsei, G. Szarka, Y. Thomann, R. Thomann, R. Mühlhaupt, B. Iván, *Materials* **2020**, *13*, 4822.
[65] I. Rombouts, B. Lagrain, K. A. Scherf, M. A. Lambrecht, P. Koehler, J. A. Delcour, *Sci. Rep.* **2015**, *5*, 12210.
[66] L. Ma, Y. Yang, J. Yao, Z. Shao, X. Chen, *Polym. Chem.* **2013**, *4*, 5425.
[67] T. A. Henderson, L. Morries, *Neuropsychiatr. Dis. Treat.* **2015**, *11*, 2191.

